Fault Detection for Proton Exchange Membrane Fuel Cell using Adaptive Extended Kalman Filter

Katherin Indriawati, Tasya Y. Christnantasari, Nur Laila Hamidah

Abstract— **One promising technique for producing electricity that is both clean and high-performing is proton-exchange membrane fuel cells or PEMFCs. It is important to diagnose the fault in the PEMFCs system to ensure its performance and safety in operation. Drying is one of the faults in PEMFCs that occurs when relative humidity drops and temperature uplift takes place simultaneously. Here, we proposed the fault detection (FD) model utilizing an adaptive extended Kalman filter (AEKF) to detect drying that affects the membrane and catalyst's proton conductivity by implementing three drying scenarios based on severity. PEMFCs were used to realize the electrochemical properties and accommodate the characteristics of drying. An AEKF was used as a residual generator and fixed threshold for the residual evaluation. The findings show that an increase in temperatures and a decrease in relative humidity representing the drying condition caused the membrane's water uptake and catalyst to drop. It further decreased the PEMFC's proton conductivity and performance. The results of the proposed FD scheme using AEKF showed that the fault detection succeeded in detecting all drying fault scenarios within less than one second.**

Index Terms— **PEM fuel cell, clean fuel technology, fault detection, Adaptive extended Kalman filter, residual generator**

I. Introduction

PEMFCs, or proton exchange membrane fuel cells plays a key development in tackling global emissions since it is a form of clean energy, which only produces heat and water as its side effects. PEMFCs can be utilized to fulfill the wide range of energy demands, from portable application to stationary power generation. This is because, in comparison to other fuel cell types, it produces great power density while having low weight and volume.

Manuscript received January 24, 2023; revised April 30, 2024.

This work was supported by the Institut Teknologi Sepuluh Nopember under project scheme of the Publication Writing and IPR Incentive Program (PPHKI).

Katherin Indriawati is a Professor in Department of Engineering Physics, Faculty of Industrial Technology and Systems Engineering, Institut Teknologi Sepuluh Nopember, Surabaya 60111, Indonesia (e-mail: katherin@ep.its.ac.id).

Tasya Y. Christnantasari is a joint researcher at Department of Electrical and Electronic Engineering, Imperial College London, London SW7 2AZ, United Kingdom (e-mail: christnantasari.tasya@outlook.com).

Nur Laila Hamidah is an Assistant Professor in Department of Engineering Physics, Faculty of Industrial Technology and Systems Engineering, Institut Teknologi Sepuluh Nopember, Surabaya 60111, Indonesia. (*corresponding author, e-mail: nurlaila@its.ac.id, nurlaila.hamidah88@gmail.com).

PEMFCs also offer relatively high efficiency, which is about 40%-60% [1]. The past few years have shown an enormous development in ensuring good performance and safe operation, it is important to diagnose the faults in the PEMFC system that can deteriorate its performance and reduce remaining useful life (RUL) [2]–[4]. Faults in the fuel cells might result in permanent damage to the system. The faults might be induced by fuel impurities, water management, aging, or component degradation. Water state has been shown as an essential influence on PEMFCs' proton conductivity and reliability, especially during normal operation. Contrarily, dehydration or drying conditions might impede the proton diffusion in the membrane [5]. Thus, water management is crucial to the PEMFC's normal operation.

Drying in PEMFCs occurs when relative humidity drops and temperature uplift takes place simultaneously during the operation [6]. Consequently, the evaporation rate will increase and drop the cell's hydration, inducing a decrease in the water uptake and proton conductivity. Furthermore, drying is represented by temperature and air pressure increase, whereas flooding is described by a constant decrease in transport of mass and the exchange of current density [7]. when the fault is not well-managed, it might form a pinhole at the proton-exchange membrane and catalyst deposition. This should be avoided by designing a fault detection system that acts as the first line of defense for PEMFCs.

Several previous studies on PEMFCs have shown significant interest in fault detection through various methods. Zhang & Pisu [8]. proposed model-based fault detection using a cascaded, unscented Kalman filter to detect flooding at the cathode side of PEMFCs. That study applied abrupt fault, which was simulated at 3,000s, and implemented voltage residual for the fault evaluation. Radial basis function (RBF) based fault detection was proposed by Kamal et al. [9] to identify and separate faults in actuators and sensors. The results demonstrated that the developed method could identify and separate different fault sizes up to +/-10%. In another study, Zhang & Pisu [10] proposed model-based fault detection using an unscented Kalman filter to detect catalyst degradation. That study briefly compared normal and faulty conditions. The results were tested with a fixed threshold. Aitouche et al. [11] offered nonlinear analytical redundancy to detect actuator and sensor faults. Laribi et al. [12] performed electrochemical impedance spectroscopy and fuzzy clustering to detect flooding, drying, and oxygen

starvation. Furthermore, Ramamoorthy & Mid [13] proposed model-based fault detection through an extended Kalman filter to detect flooding and drying faults. This study implemented parameter changes simulated at 4s as a representation of existing faults.

A novel approach of the extended Kalman filter was introduced to calculate the non-linear system state and to diagnose the sensor's faults. However, its estimation is not optimal due to inaccurate information on noise statistics resulting in degrading diagnostic performance. Hence, the development of an adaptive extended Kalman filter (AEKF) has been proposed to address the issue regarding the covariance matrices of the measurement and process noises that dynamically modify their magnitude [5], [14].

Based on previous studies, this paper proposed an FD design for PEMFCs to detect drying that affects the membrane and catalyst's proton conductivity. The model was based on an AEKF, which functioned as a residual generator and with a fixed threshold for the residual evaluation. In addition, this paper implemented three drying scenarios based on severity. Finally, to verify the detection performance in the suggested scheme, a numerical analysis was conducted. The parameter values used in this study referred to several previous studies [1], [15]–[21] (Table 1). These variables are applied to calculate PEM fuel cells` performance and to model their dynamics.

II. PEMFC MODELING

To implement model-based FD, the PEMFC model is required to identify electrochemical properties and describe the fault. The required model is needed to accommodate and capture the drying characteristics. In this case, dynamic equations highlighted the PEMFC's temperature and relative humidity since those are the main perceptible aspects of drying. The membrane examined in this study was based on the Nafion membrane characteristics. To simplify PEMFCs' dynamic model, several assumptions were considered such as All gases complied with the ideal gas law and were equally distributed and the anode and cathode temperature is the same as the stack temperature.

A. Open Circuit Voltage of PEMFC

For PEMFC, an anode and a cathode are sandwiched with a proton exchange membrane, which is a platinum-carbon catalyst coated on the anode and cathode side[14]. Hydrogen as the fuel is pumped to the anode, while oxygen is supplied as the reducing agent at the cathode. Due to the presence of the catalyst, protons (H^+) and electrons (e^-) are generated at the anode side by the oxidation of hydrogen. The proton-exchange membrane acts as the semipermeable membrane that only allows protons (H^{+}) to pass through to the cathode from the anode. The electrons cross from the anode to the cathode by going through an external circuit, resulting in the production of electrical current. Water, which remains as the residue of the PEMFC, is produced by the recombination of protons, electrons, and oxygen on the cathode. The oxidation reaction that occurred at the cathode and the reduction reaction that occurred at the anode are described below:

$$H_2 \rightarrow 2H^+ + 2e^- \quad (1)$$

$$O_2 + 4H^+ + 4e^- \rightarrow 2H_2O \quad (2)$$

TABLE I
PEMFC PARAMETERS

Parameter (Unit)	Symbol	Values
Water diffusion coefficient (m^2/s)	dw	2.1×10^{-7}
Membrane thickness (m)	t	2.54×10^{-6}
Universal gas constant (J/K.mol)	R	8.3144
Faraday constant (C/mol)	F	96.485
Number of acid groups filled with water	C	1.8844
Relative humidity of half physisorption binding sites (%).	φ_i	94.190
Langmuir equilibrium constant	K	5.517
Temperature dynamic constant	α	6.41×10^{2}
	β	1.4×10^{-1}
	γ	1.21×10^{-1}
PEMFC active area (cm^2)	AC	$5.,84 \times 10^{-2}$
Cell number	N	1
Cathode thickness (μm)	$\delta_{cathode}$	4.5
Anode thickness (μm)	δ_{anode}	2.8
Ionomer volume fraction of the cathode	ε_{cat}	0.17
Ionomer volume fraction of the anode	ε_{an}	0.19
Volume fraction constant	n	2
Mass flowrate input to the cathode (l/s)	$Cathode_{in}$	0.05
Mass flowrate output from the anode (l/s)	$Anode_{in}$	0.167
H_2 mol fraction	YH_2	0.99
O_2 mol fraction	YO_2	0.21
Sulphonic group concentration (mol/m^3)	a	1200
Reference temperature (K)	T_0	303.15
Current (mA)	I	1.2

The following equation is applied to calculate the reversible electric potential of PEMFCs using the change in Gibb's free energy [22]:

$$V_{o,fc} = n_{cell}\left(-\frac{CE}{2F}\right) \quad (3)$$

where $V_{O,fc}$ is open circuit voltage of PEMFCs, n_{cell} denotes the number of cells, CE indicates the shift of Gibb's free energy, and F represents the constant of Faraday. A shift in Gibb's free energy is obtained through [14].

$$\Delta G = \Delta G^0 - RT\ln\left(\frac{P_{H_2}\sqrt{P_{O_2}}}{P_{H_2O}}\right) \quad (4)$$

where ΔG^0 is a shift in Gibb's free energy under typical operational settings, R and T ar gas constant and temperature, P_{H_2}, P_{O_2}, and P_{H_2O} denote partial pressure of hydrogen, oxygen, and water. Substituting Equation (4) with Equation (3)

$$V_{O,fc} = n_{cell}\left(-\frac{\Delta G^0}{2F} + \frac{RT}{2F}\ln\left(\frac{P_{H_2}\sqrt{P_{O_2}}}{P_{H_2O}}\right)\right) \quad (5)$$

Equation (5) can be rewritten as

$$V_{O,fc} = n_{cell}\left(E^{0}_{cell} + \frac{RT}{2F}\ln\left(\frac{P_{H_2}\sqrt{P_{O_2}}}{P_{H_2O}}\right)\right) \quad (6)$$

Where E^{o}_{cell} is reference potential at standard operating conditions.

B. Irreversible Voltage Losses in PEMFCs

The actual voltage of the PEMFC depends on the irreversible voltage losses, called polarization, which take place within the PEMFC [13]. Ohmic losses, concentration losses, and activation losses are the three primary types of losses that are usually observed in PEMFC. Activation losses can occur due to the gradual electrode kinetics that arise from the rate at which electrochemical reactions take place on an electrode's surface[13]. These losses have crucial effects on low current densities, particularly at the beginning of the polarization curve. The losses associated with the activation of single-cell PEMFCs is modeled as follows [23]:

$$V_{act} = \frac{RT}{2F}\ln\left(\frac{I}{I_d}\right) = a_0 + T\left[a + b\ln I\right] \quad (7)$$

where V_{act} is activation losses, I and I_d denote the current and current density, a_0, a, and b are constants in the Tafel equation.

Ohmic losses are evoked by the PEMFC's ohmic resistance. This includes the resistance of all components, anodes, cathodes, and membranes because of shortcomings in the production process and resistance of the ions' mobility [14]. PEMFC's ohmic resistance can be written as follows:

$$V_O = IR_O = V_O^A + V_O^C + V_O^M = I(R_O^A + R_O^C + R_O^M) \quad (8)$$

where V_0 represents ohmic losses, and R_0 is the ohmic resistance. The superscript A, C, and M represent the ohmic losses and ohmic resistance at the anode, cathode, and membrane respectively. Concentration losses take place because of the emergence of reactants' concentration gradient at the electrode's surface [14]. The concentration losses for PEMFC can be given as follows:

$$V_{conc} = \frac{RT}{eF}\ln\left(1 - \frac{I}{I_L}\right) \quad (9)$$

where V_{conc} is the concentration loss, e is the quantity of electrons involved, and I_L denotes a limiting current. Thus, the actual voltage output of PEMFCs is gained by calculating the deviation between overall losses and the open circuit voltage of the PEMFC.

$$V_{fc} = V_{O,fc} - n_{cell}\left(V_{act} - V_O - V_{conc}\right) \quad (10)$$

C. Dynamic Equations of PEMFC

Pressure is operated on the cathode and anode. The partial pressure of oxygen is represented by the cathode, whereas the anode indicates the hydrogen partial pressure. The water pressure is included as well in the calculation. The dynamic model of partial pressures is presented by applying the conservation of mole rule and ideal gas law. According to those concepts, the value of each partial pressure is determined by the total rate at which gas flows [23]. The equations describing the change in hydrogen and oxygen partial pressure are given by [23]:

$$\frac{dP_{H_2}}{dt} = \frac{RT}{V_A}\left(\dot{m}_{H_2,in} - \dot{m}_{H_2,rea} - \dot{m}_{H_2,out}\right) \quad (11)$$

$$\frac{dP_{O_2}}{dt} = \frac{RT}{V_A}\left(\dot{m}_{O_2,in} - \dot{m}_{O_2,rea} - \dot{m}_{O_2,out}\right) \quad (12)$$

where P_{H_2}, P_{O_2} $\dot{m}_{H_2}$ $\dot{m}_{O_2}$ denote the hydrogen and oxygen partial pressure, the hydrogen mass, and the oxygen mass, respectively. The subscripts in, out, rea, and gen represent the mass flow rates of the corresponding variables at the inlet, outlet, reacted, and generated points.

At the outlet, the mass flow rates of oxygen and hydrogen are represented as:

$$\dot{m}_{H_2,out} = \dot{m}_{H_2,in}\left(\frac{2P_{H_2} - P_A}{P_A}\right) \quad (13)$$

$$\dot{m}_{O_2,out} = \dot{m}_{O_2,in}\left(\frac{2P_{O_2} - P_C}{P_C}\right) \quad (14)$$

where P_C and P_A are cathode and anode pressure.

The reacted and generated flow rate of each fuel can be obtained through:

$$\dot{m}_{H_2,rea} = \frac{n_{cell}I}{2F} \quad (15)$$

$$\dot{m}_{O_2,rea} = \frac{n_{cell}I}{4F} \quad (16)$$

where n_{cell} is numbers of cells, I is current, and F is the Faraday constant.

The inlet mass flow rate can be given as follows:

$$\dot{m}_{H_2,in} = \frac{m_{H_2O^a_{in}}}{P_{H_2O^a_{in}}} \quad (17)$$

$$\dot{m}_{O_2,in} = \frac{m_{H_2O^c_{in}}}{P_{H_2O^c_{in}}} \quad (18)$$

where $m_{H_2O^a_{in}}$ and $m_{H_2O^c_{in}}$, $P_{H_2O^a_{in}}$ and $P_{H_2O^c_{in}}$ represent the inlet mass flow rate and inlet water pressure at the anode and cathode, respectively.

The dynamics of water's partial pressure depend on the net water flow rate over the membrane and the water formation during the reaction, as given below:

$$\frac{dP_{H_2O}}{dt} = \frac{RT}{V_C}\left(2\frac{m_{H_2O^c_{in}}\left(P^{in}_{H_2O} - P_{H_2O}\right)}{P_{H_2O^c_{in}}} - 2\frac{1}{4F}I\right) \quad (19)$$

where P_{H_2O} is water partial pressure and $P^{in}_{H_2O}$ denotes inlet water pressure.

The dynamic of relative humidity depends on water's partial pressure since the ratio between the partial pressure of water and its saturated pressure is known as relative humidity. It can be expressed as [24]

$$\frac{dRH}{dt} = \frac{RT}{V_C P_{sat}}\left(2\frac{m_{H_2O^c_{in}}\left(P^{in}_{H_2O} - P_{H_2O}\right)}{P_{H_2O^c_{in}}} - 2\frac{1}{4F}I\right) \quad (20)$$

where P_{sat} is saturated pressure.

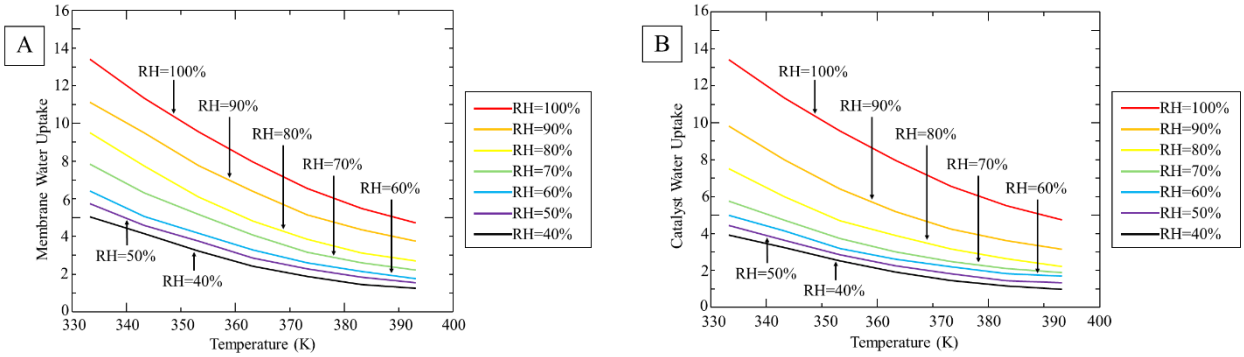

Fig. 1. The dependent of temperature and RH on the water uptake of (A) Membrane (B) Catalyst

$$\frac{dT}{dt} = \left[\frac{h_s n_{cell} A_{fc}}{M_{fc} C_{fc}}\right] T - \left(n_{cell}\left[\left(\frac{E^0_{cell}}{M_{fc} C_{fc}}\right) + \left(\frac{RT}{F M_{fc} C_{fc}}\right) ln\left(\frac{P_{H_2}\sqrt{P_{O_2}}}{P_{H_2O}}\right) - V_{act} - V_{cocn} - V_O\right]\right) 1 + \left[\frac{h_s n_{cell} A_{fc}}{M_{fc} C_{fc}}\right] T_R \qquad (21)$$

Temperature dynamics depend on the heat generated in the PEMFCs, which can be any form of heat generation. This includes heat generation during electrochemical reactions, heat generation due to electrical output power, and heat generation because of air convection. The temperature dynamic equation as in Eq.21. Where A_{fc} is the area of active cells and h_s is the convective heat transfer coefficient, M_{fc} is fuel cell mass, C_{fc} denotes molar heat capacity, and T and T_R represent temperature and ambient temperature.

III. Draying Faults PEMFCS

Based on the review of PEMFC drying in previous works [25], drying is one of the most common faults that occurs during the operation process. Drying is induced by water management faults. It takes place if humidification decreases, and temperature increases simultaneously. In this paper, the effects of both parameters were further studied through simulations of the PEMFC model. This was done to get an insight into the severity of the possible drying faults in PEMFC.

Among the most significant aspects of the PEMFC is temperature. since it has a direct influence on several PEMFC variables such as water uptake, proton conductivity, and resistance. When the temperature uplift takes place, it lowers the catalyst's and membrane's water uptake as shown in Fig 1. The increasing temperature evokes the deformation of the Nafion membrane's fluoro-backbone. This further results in a decrease of the sulfonic group, which leads to a reduction in membrane and catalyst water absorption [26]. Moreover, this tends to slowly dispose of and dissolve the Pt molecule of the catalyst in the membrane. This results in H_2O_2 or radical generation and membrane degradation, which could hinder the proton transport inside the membrane [27], as seen in Fig 1. High temperatures also tend to quicken catalyst degradation. This then reduces the catalyst layer's water absorption at the sulfonic-acid moieties and further drops the catalyst's water uptake. If this condition is not well-managed, this could cause permanent damage to the catalyst, and even result in catalyst delamination [28].

Relative humidity also has an essential role in the PEMFC. As reflected by Fig 1, the membrane and catalyst water are affected by relative humidity. The PEMFC's relative humidity represents water molecules that are absorbed by the hydrophilic sulfonic-acid group and directly related to water uptake. When relative humidity drops, this indicates a decrease in absorbed water molecules and leads to a drop in water uptake.

The increasing temperature also leads to rising membrane resistance, as shown in Fig 2. High temperatures cause the removal of some sulfonic acid groups in the membrane, which impedes proton transport and increases membrane resistance. The increase of resistance causes the ohmic losses in the membrane and further results in increased irreversible PEMFC voltage. Thus, it influences the PEMFC system's performance.

The effects of temperature uplift on proton conductivity is depicted in Figure 3. The effect is notably greater in the catalyst. When temperature increases, the number of sulfonic acid groups decreases due to the distortion of fluoro-backbone in the Nafion membrane forming protonated water ($(H)^+H_2O$). This phenomenon diminishes the membrane and catalyst's proton transport [29]. As a result, there is a loss of proton conductivity. The prolonged temperature uplift could result in permanent damage to both the membrane and catalyst.

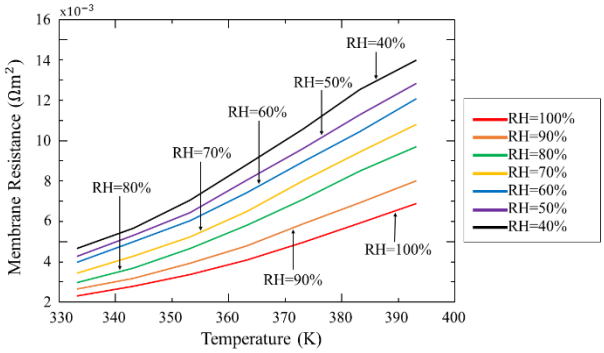

Fig. 2. The dependence of temperature and RH on membrane resistance

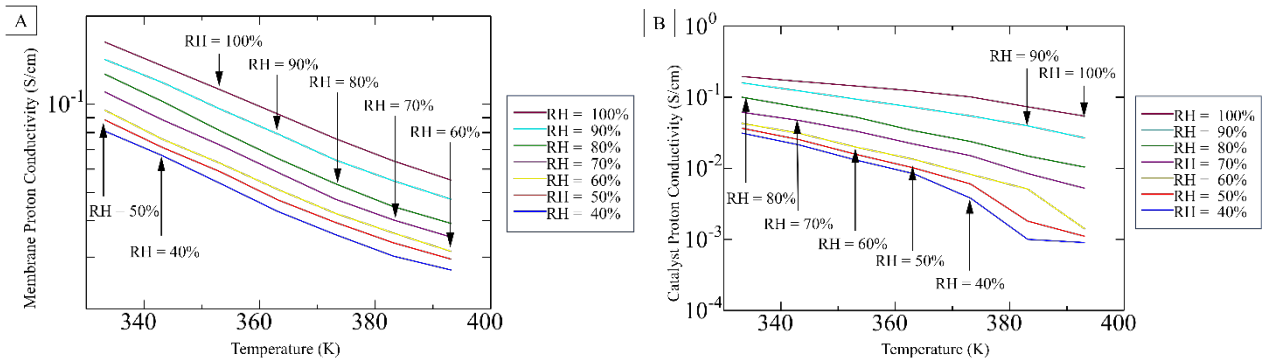

Fig. 3 The temperature and RH dependence on proton conductivity of (A) Membrane (B) Catalyst

$$\begin{bmatrix} x_{1_{k+1}} \\ x_{2_{k+1}} \\ x_{3_{k+1}} \\ x_{4_{k+1}} \end{bmatrix} = \begin{bmatrix} -\frac{1}{\alpha}\left(x_{1_k} - T_0\right) + \frac{\beta}{\alpha}u_1 + \frac{\gamma}{\alpha}u_1^2 \\ M_{H_2O}N\frac{n_d u_1}{F} - M_{H_2O}A_c\frac{D_{H_2O}\left(x_{2_k}\right)}{t} \\ \frac{R.x_{1_k}}{V_A}\left(Y_{H_2}u_2 - 2K_rU_1 - \left(u_2 - 2K_rU_1\right)\frac{x_{3_k}}{P_{op}}\right) \\ \frac{R.x_{1_k}}{V_C}\left(Y_{O_2}u_3 - 2K_rU_1 - \left(u_3 - K_rU_1\right)\frac{x_{4_k}}{P_{op}}\right) \end{bmatrix} \tag{22}$$

$$y_k = 1.229 - 0.85\times10^{-3}\left(x_{1_k} - 298.15\right) + 4.310\times10^{-5}x_{1_k}.\left[\ln\left(x_{3_k}\right) + 0.5\ln\left(x_{4_k}\right)\right] + \frac{Rx_{1_k}}{2F}\ln\left(\frac{x_{2_k}}{100\%}\right) - \frac{R_m u_1}{A_c} - \frac{\vartheta_{anode}}{A_c 2\sigma\varepsilon^n}u_1 - \frac{\vartheta_{cathode}}{A_c 2\sigma\varepsilon^n}u_1 \tag{23}$$

Temperature and humidity are two of the factors used to determine the fuel system's design parameters as described in [30]. However, no matter how good the value of the fuel cell system's design parameters and their supporting components, good system performance cannot be achieved if there is an error resulting in the PEMFC temperature and humidity not being maintained at the set values. For this reason, a fault detection system, such as drying fault detection, is needed to give an early warning before a total fuel cell system failure occurs.

IV. Proposed Fault Detection Scheme

A model-based FD strategy for the PEMFC is provided in this section. A process model of a PEMFC was needed to capture the PEMFC process's dynamics. In addition, the model output was able to be utilized to produce the residuals by comparing the model output with the measured output. Nonetheless, the residual may have had some noises due to disturbance, model inaccuracy, and unknown initial conditions. Observer-based fault detection, which addresses these problems, was implemented by substituting the state observer for the model and residual generator. [31].

The AEKF, a state observer that operated in line with the PEMFC system, used the observed voltage and current input to identify any drying faults in the PEMFC. The system states were estimated and further applied to estimate the voltage output. The residual was obtained by subtracting the estimated voltage of the AEKF from the measured voltage of the PEMFC system. Eventually, the residual evaluation was implemented to identify drying faults. The schematics of the proposed fault detection system are depicted in Fig 4.

The AEKF algorithm operated based on the reviewed plant. According to the PEMFC modeling discussed in Section II, the equation representing the nonlinear PEMFC model was formulated in the state space format. This was achieved by examining four state variables, consisting of one output variable and three input variables. The definitions of these variables are provided as follows:

x_1 = temperature (K)
x_2 = relative humidity (RH) (%)
x_3 = hydrogen partial pressure (Pa)
x_4 = oxygen partial pressure (Pa)
y_k = output voltage (Ecell) (V)
u_1 = current (mA)
u_2 = Anodein (l/s)
u_3 = Cathodein (l/s)

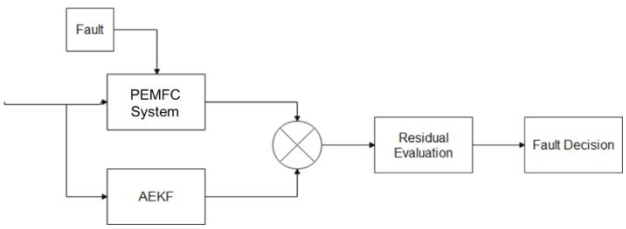

Fig. 4. Proposed Fault Detection Schemes

The equation representing the PEMFC's dynamic model in the discrete time domain at time step k is as in Eq.22 – Eq.23.

A. AEKF Algorithm

The AEKF offers adaptive tuning of process and

measurement noise covariance matrices. This brief study implemented the voltage residual covariance matching method, which indicates that voltage residual is the parameter which adaptively tunes the noise covariance matrices. The AEKF algorithm can be summarized as follows [31]:

Define the following state space model

$$\begin{cases} x_{k+1} = f\left(x_k, u_k\right) + w_k \\ y_k = h\left(x_k, u_k\right) + v_k \end{cases} \tag{24}$$

and Jacobian matrices

$$F_{k-1} = \left.\frac{\partial f\left(x_k, u_k\right)}{\partial x}\right|_{\hat{x}_{k-1}} \tag{25}$$

$$H_k = \left.\frac{\partial h\left(x_k, u_k\right)}{\partial x}\right|_{\hat{x}_{k|k-1}} \tag{26}$$

Initialization

For $k = 0$, set $x_0^+ = E\left[x_0\right]$,

$$P_0^+ = E\left[\left(x_0 - x_0^+\right)\left(x_0 - x_0^+\right)^T\right], Q_o, R_0$$

Time Update

A priori start estimate update

$$\hat{x}_{k|k-1} = f\left(\hat{x}_{k|k-1}, u_{k-1}\right) \tag{27}$$

A priori error covariance estimate update

$$P_{k|k-1} = F_{k-1} P_{k-1} F_{k-1}^T + Q_{k-1} \tag{28}$$

Measurement and Noises update

Innovation update

$$d_k = z_k - h\left(\hat{x}_{k|k-1}, u_{k-1}\right) \tag{29}$$

Kalman gain update

$$K_k = P_{k|k-1} H_k^T + \left(H_k P_{k|k-1} H_k^T + R_{k-1}\right)^{-1} \tag{30}$$

A posterior state estimate update

$$\hat{x}_k = \hat{x}_{k|k-1} + K_k\left[d_k\right] \tag{31}$$

A posterior error covariance estimate update

$$P_k = \left(I - K_k H_k\right) P_{k|k-1} \tag{32}$$

Residual update

$$\varepsilon_k = z_k - h\left(\hat{x}_k, u_k\right) \tag{33}$$

Process noise covariance update

$$C_{\varepsilon_k} = \frac{1}{N}\sum_{j=j0}^{k} \varepsilon_j \varepsilon_j^T \tag{34}$$

$$Q_k = K_k \hat{C}_{\varepsilon_k} K_k^T \tag{35}$$

Where the Jacobian matrix during time step k-1 is denoted by F_{k-1}, the observation matrix during time step k is represented by H_k, $\hat{x}_{k|k-1}$ is a representation of the state of a priori estimated during time step k, the calculated the error covariance of a priori during time step k is denoted by $P_{k|k-1}$, the state of a posteriori estimated during time step k is denoted by $\hat{x}_k$, the calculated error covariance of a posteriori during time step k is denoted by P_k, Kalman gain during time step k is denoted by K_k, the covariance matching window size is N, the residual of voltage during time step k is denoted by ε_k, and the voltage residual's covariance during time step k is estimated by $\hat{C}_{\varepsilon_k}$.

The state space function (24) is defined in relation to equations (22) and (23), such that the Jacobian matrix is obtained using formulas (25) and (26) and can be expressed as in Eq.36 – Eq.37. Where VA is anode volume, V_C is cathode volume, and K_r is the ratio between the cell and Faraday constant. Y_{H_2} and Y_{O_2} are H_2 and O_2 mol fraction, D_λ is back diffusion coefficient, t is membrane thickness, P_{op} is operation pressure, and A_c is active cell area.

$$F_k = \begin{bmatrix} -\frac{1}{\alpha} & 0 & 0 & 0 \\ 0 & m_{h_2O} A_c \frac{D\lambda}{t} & 0 & 0 \\ \frac{R}{V_A}\left(Y_{H_2} u_2 - 2K_r u_1 - \left(u_2 - 2K_r u_1\right)\frac{\hat{x}_{3_{k-1}}}{P_{op}}\right) & 0 & -\frac{R.\hat{x}_{1_{k-1}}}{V_A}\left(u_2 - 2K_r u_1\right)\frac{1}{P_{op}} & 0 \\ \frac{R}{V_c}\left(Y_{O_2} u_2 - 2K_r u_1 - \left(u_3 - K_r u_1\right)\frac{\hat{x}_{4_{k-1}}}{P_{op}}\right) & 0 & 0 & -\frac{R.\hat{x}_{1_{k-1}}}{V_A}\left(u_2 - 2K_r u_1\right)\frac{1}{P_{op}} \end{bmatrix} \tag{36}$$

$$H_k = \left[-0.85\times10^{-3} + 4.31\times10^{-5}.\left[\ln\left(\hat{x}_{3_{k|k-1}}\right) + 0.5\ln\left(\hat{x}_{4_{k|k-1}}\right)\right] + \frac{R}{2F}\ln\frac{\hat{x}_{2_{k|k-1}}}{100\%}\frac{R\hat{x}_{1_{k|k-1}}}{2F\hat{x}_{2_{k|k-1}}}\frac{4.31\times10^{-5}\hat{x}_{1_{k|k-1}}}{\hat{x}_{3_{k|k-1}}}\frac{4.31\times10^{-5}\hat{x}_{1_{k|k-1}}}{\hat{x}_{4_{k|k-1}}}\right] \tag{37}$$

B. Residual Evaluation

This study utilized AEKF-based fault detection to detect drying faults. In this case, the AEKF functioned as a residual generator. The residuals were produced by the distinction between the measured and estimated output voltage that is expressed as:

$$r_{V_T} = y_{V_T} - \hat{V}_{T_t} \tag{38}$$

Where r_{V_T} is the voltage residual of PEMFC, $\hat{V}_{T_t}$ and y_{V_T} stand for the measured and estimated output voltage of PEMFC, correspondingly.

Drying faults were detected by seeing when the residual value became greater than the threshold. The utilized threshold was a fixed threshold, which was set to be higher than the AEKF's acceptable standard deviation in normal (fault-free) conditions to prefent any false alarms. The designated threshold was four times the residual's standard deviation under normal conditions (no errors). The fault detection system that was designed was:

$$d = \begin{cases} 1 & r(k) < -4\sigma \\ 0 & r(k) \geq -4\sigma \end{cases} \tag{38}$$

With:

d	=	detection
$r(k)$	=	Residual on k
σ	=	standard deviation under normal conditions

A negative threshold occurs due to voltage drops caused by drying mistakes, leading to the generation of negative residuals. The digit "1" in the detection signifies a drying error in the PEMFC, whereas the digit "0" indicates that the PEMFC is operating under normal conditions.

This brief study implemented three scenarios based on temperature and relative humidity conditions. Table 2 presents an overview for each of these scenarios. According to the results of simulation in Section 3, drying worsened from Variation #1 to Variation #3. This was related to the degradation ratio of water uptake, membrane resistance, and catalyst conductivity, with respect to non-faulty conditions. Those scenarios were considered as abrupt faults. Each variation was simulated as an abrupt change to the PEMFC model affecting the system's state, which further influenced the output voltage. This resulted in differences between the measured and estimated voltage values.

TABLE II
DRYING FAULT SCENARIOS

Parameter	Non-faulty condition	Drying Variation #1	Drying Variation #2	Drying Variation #3
Temperature (K)	333.15	363.15	378.15	393.15
Relative Humidity (%)	100	70	50	30
Membrane water uptake degradation (%)	0	68.1	82.6	86.9
Membrane resistance degradation (%)	0	85.7	138.1	185.7
Catalyst conductivity degradation (%)	0	88.9	98.3	99.7

V. RESULT AND DISCUSSION

Before implementing the FD algorithm, trial and error experiments were used to determine the window size N, noise covariance Q_0 and R_0, and initial error covariance P_0 for the covariance matrix of the AEKF algorithm. The test results recommended the best value of those parameters were:

$$P_0 = \begin{bmatrix} 0.01 & 0 & 0 & 0 & 0 \\ 0 & 0.01 & 0 & 0 & 0 \\ 0 & 0 & 0.01 & 0 & 0 \\ 0 & 0 & 0 & 0.01 & 0 \\ 0 & 0 & 0 & 0 & 0.01 \end{bmatrix}$$

$$Q_0 = \begin{bmatrix} 0.0001 & 0 & 0 & 0 & 0 \\ 0 & 0.0003 & 0 & 0 & 0 \\ 0 & 0 & 0.0003 & 0 & 0 \\ 0 & 0 & 0 & 0.0001 & 0 \\ 0 & 0 & 0 & 0 & 0.0005 \end{bmatrix}$$

$$R_0 = 0.00001$$

$$N = 100$$

The AEKF's function within the residual generator suggested that the AEKF should serve as a model of the system under normal conditions. Consequently, the AEKF was initially tested under uninterrupted conditions.

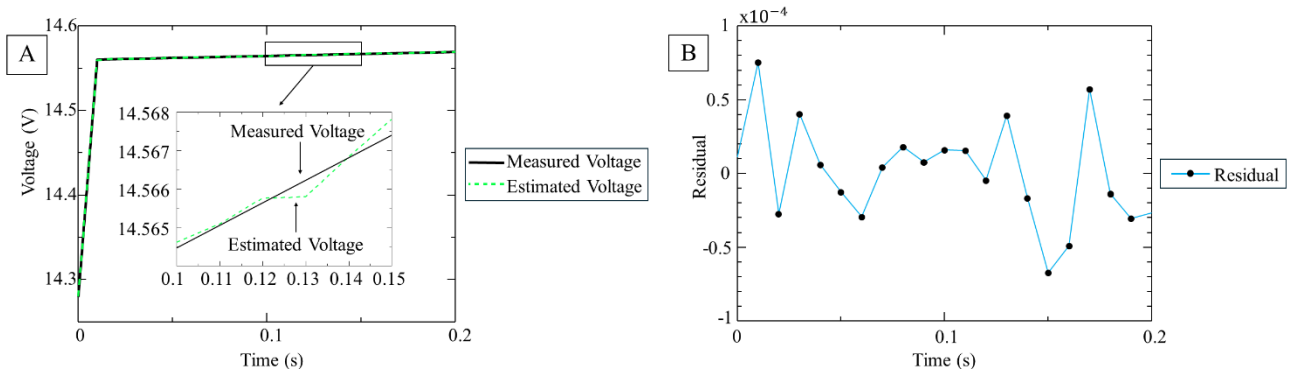

Fig. 5. The AEKF algorithm test results: (A) the estimated voltage compared to measured voltage (B) Residual signal.

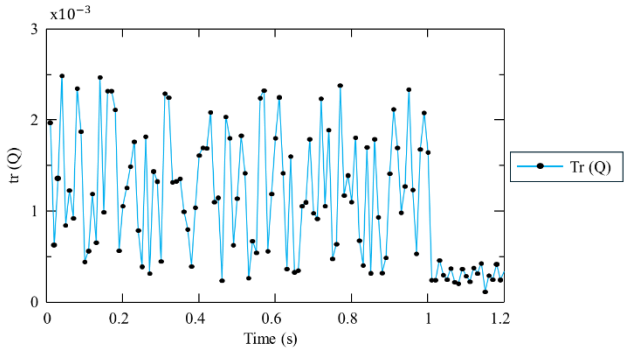

Fig. 6. Change in trace value of process noise covariance, tr(Q)

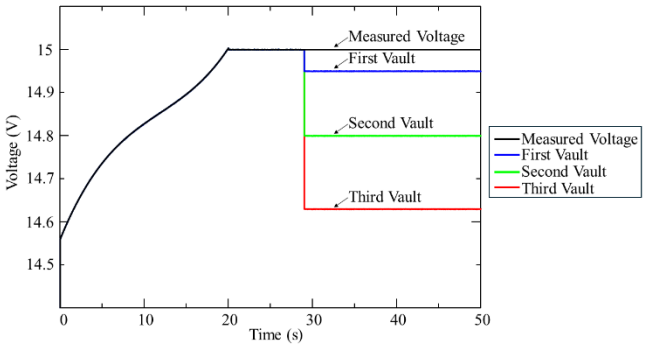

Fig. 7. The dependence of temperature and RH on membrane resistance

This test aimed to evaluate the accuracy of the AEKF model in accurately representing normal or uninterrupted operating conditions in the PEMFC. Fig. 5 illustrates the test results. Fig 5A demonstrates that the AEKF converged the measured voltage at less than 0.01s and had an RMSE of 5.7 x $10^{-5.}$ Fig 5B displays the corresponding residual value. The residual value under normal conditions was close to zero, indicating that the AEKF was capable of accurately estimating the PEMFC's output voltage. The standard deviation for this signal was about 0.0032. Using (39), the threshold was determined to be -0.0128.

The AEKF technique allows changes in the matrix value of covariance on the process noise Q following (35). Fig. 6 shows how the trace Q values dynamically fluctuate. This characteristic relates to the adaptive nature of AEKF proposed in this study. After one second, the value of tr(Q) stabilizes at a value below 0.5 x 10^{-3}, after having fluctuated due to the initial conditions.

Table 3 displays the simulation outcomes for the initial fault conditions. As can be observed, the residual value always surpassed the cutoff of -0.0128, enabling the identification of any faults. However, the duration required to identify each type of fault differs. The residual size and detection time increased in proportion to the error size.

The AEKF results for the first, second, and third fault scenarios (drying variations #1, #2, and #3, respectively) injected at 30s are depicted in Fig 7. Drying caused the voltage to have a lower magnitude. When the fault was injected, the measured voltage dropped, and this created a discrepancy between the AEKF's measured output and estimated output. This difference led to a residual uplift. It can also be seen that the #3 residual had maximum discrepancy compared to the other residuals, which further implies that the severity of faults influences the voltage drop.

The residual values for the three fault scenarios are shown in Table 4. From those results, it is proven that the

TABLE III
RESIDUAL VALUES FOR FAULT SCENARIOS INJECTED AT 0S

Parameter	Drying Variation #1	Drying Variation #2	Drying Variation #3
Residual	-0.033	-0.058	-0.097
Time Detection	0.35s	0.17s	0.01s

greater the severity, the greater the residual. Moreover, the fault detection succeeded in detecting all drying faults within less than 1s. It can be seen that the greater the severity, the sooner the faults were detected.

The detection times in Table 3 and Table 4 have varying values. A longer detection time was required when the fault was introduced at the beginning of the simulation because the AEKF was still proceeding towards a steady state from the initial condition. The AEKF was in a steady state when the fault was introduced at 30 seconds.

It is demonstrated in Section III that changes in temperature and humidity values can be used to indicate drying conditions. Therefore, by using AEKF, these two variables are estimated as x_1 and x_2. However, the detection system built was very dependent on the fuel cell model. Even though it had adaptive features, the AEKF's performance could still decrease if the reference model differed greatly from the real plant. To overcome this, a data-based fault detection algorithm can serve as an alternative solution. Data-based fault detection algorithms have been described in [32]. Previous studies indicate that they can be used even if the amount of data available is small.

TABLE IV
RESIDUAL VALUES FOR FAULT SCENARIOS INJECTED AT 30S

Parameter	Drying Variation #1	Drying Variation #2	Drying Variation #3
Residual	0.07	0.16	0.35
Time Detection	0.1s	0.08s	0.0001s

VI. CONCLUSION

Drying conditions as fault detection representation in PEMFC have been examined using an AEKF. Drying occurred when the temperature increased, and relative humidity decreased simultaneously. The PEMFC's characteristics were modelled to realize drying as a fault in the system. The results suggest that drying led to a decrease in the water absorption of the membranes and catalyst. This impeded proton transport in the membrane, leading to loss of proton conductivity in the PEMFC. A proposed FD scheme using an AEKF was presented in this study. The proposed FD scheme was tested using three scenarios based on the severity of the drying faults. The results indicate that the FD scheme successfully identified any scenario in below 1s.

REFERENCES

[1] Z. Abdin, C. J. Webb, and E. MacA. Gray, "PEM fuel cell model and simulation in Matlab–Simulink based on physical parameters," Energy, vol. 116, pp. 1131–1144, Dec. 2016.

[2] J. Han, J. Han, and S. Yu, "Experimental analysis of performance degradation of 3-cell PEMFC stack under dynamic load cycle," International Journal of Hydrogen Energy, vol. 45, no. 23, pp. 13045–13054, Apr. 2020.

[3] Y. Shao, G. Yin, and Y. Gao, "Understanding and approaches for the durability issues of Pt-based catalysts for PEM fuel cell," Journal of Power Sources, vol. 171, no. 2, pp. 558–566, Sep. 2007.

[4] L. Luo, B. Huang, Z. Cheng, and Q. Jian, "Rapid degradation characteristics of an air-cooled PEMFC stack," International Journal of Energy Research, vol. 44, no. 6, pp. 4784–4799, May 2020.

[5] P. Ren, P. Pei, Y. Li, Z. Wu, D. Chen, S. Huang, and X. Jia, "Diagnosis of water failures in proton exchange membrane fuel cell with zero-phase ohmic resistance and fixed-low-frequency impedance," Applied Energy, vol. 239, pp. 785–792, Apr. 2019.

[6] T. J. Bvumbe, P. Bujlo, I. Tolj, K. Mouton, G. Swart, S. Pasupathi, and B. G. Pollet, "Review on management, mechanisms and modelling of thermal processes in PEMFC," Hydrogen and Fuel Cells, vol. 1, no. 1, pp. 1–20, April. 2016.

[7] D. A. McKay, J. B. Siegel, W. Ott, and A. G. Stefanopoulou, "Parameterization and prediction of temporal fuel cell voltage behavior during flooding and drying conditions," Journal of Power Sources, vol. 178, no. 1, pp. 207–222, Mar. 2008.

[8] X. Zhang and P. Pisu, "An Unscented Kalman Filter Based on-line Diagnostic Approach For PEM Fuel Cell Flooding," IJPHM, vol. 5, no. 1, Nov. 2020.

[9] M. M. Kamal, D. W. Yu, and D. L. Yu, "Fault detection and isolation for PEM fuel cell stack with independent RBF model," Engineering Applications of Artificial Intelligence, vol. 28, pp. 52–63, Feb. 2014.

[10] X. Zhang and P. Pisu, "Prognostic-oriented Fuel Cell Catalyst Aging Modeling and Its Application to Health-Monitoring and Prognostics of a PEM Fuel Cell," IJPHM, vol. 5, no. 1, Nov. 2020.

[11] A. Aitouche, S. C. Olteanu, And B. O. Bouamama, "A Survey of Diagnostic of Fuel Cell Stack Systems," IFAC Proceedings Volumes, vol. 45, no. 20, pp. 84–89, Jan. 2012.

[12] S. Laribi, K. Mammar, Y. Sahli, and K. Koussa, "Analysis and diagnosis of PEM fuel cell failure modes (flooding & drying) across the physical parameters of electrochemical impedance model: Using neural networks method," Sustainable Energy Technologies and Assessments, vol. 34, pp. 35–42, Aug. 2019.

[13] D. Ramamoorthy and E. Che Mid, "Fault detection for PEM fuel cell using kalman filter," J. Phys.: Conf. Ser., vol. 1432, no. 1, p. 012070, Jan. 2020.

[14] A. L. Dicks and D. A. J. Rand, Fuel Cell Systems Explained. Wiley, Mar. 2018, pp. 1 – 468.

[15] P. Berg, K. Promislow, J. St. Pierre, J. Stumper, and B. Wetton, "Water Management in PEM Fuel Cells," Journal of The Electrochemical Society, vol. 151, no. 3, p. A341, Jan. 2004.

[16] N. H. Jalani, P. Choi, and R. Datta, "TEOM: A novel technique for investigating sorption in proton-exchange membranes," Journal of Membrane Science, vol. 254, no. 1, pp. 31–38, Jun. 2005.

[17] S. Pasricha and S. R. Shaw, "A dynamic PEM fuel cell model," IEEE Transactions on Energy Conversion, vol. 21, no. 2, pp. 484–490, Jun. 2006.

[18] A. Kosakian, L. P. Urbina, A. Heaman, and M. Secanell, "Understanding single-phase water-management signatures in fuel-cell impedance spectra: A numerical study," Electrochimica Acta, vol. 350, p. 136204, Aug. 2020.

[19] K. C. Neyerlin, H. A. Gasteiger, C. K. Mittelsteadt, J. Jorne, and W. Gu, "Effect of Relative Humidity on Oxygen Reduction Kinetics in a PEMFC," Journal of The Electrochemical Society, vol. 152, no. 6, p. A1073, Apr. 2005.

[20] Lu-Ying Chiu, B. Diong, and R. S. Gemmen, "An improved small-signal model of the dynamic behavior of PEM fuel cells," IEEE Transactions on Industry Applications, vol. 40, no. 4, pp. 970–977, Aug. 2004.

[21] Bei Gou, Woonki Na, and Bill Diong, "Linear and Nonlinear Models of Fuel Cell Dynamics," in Fuel Cells: Dynamic Modeling and Control with Power Electronics Applications, CRC Press, Jan. 2017, pp. 1 – 393.

[22] M. H. Nehrir and C. Wang, Modeling and Control of Fuel Cells: Distributed Generation Applications. Wiley, Mar. 2009, pp. 1 - 296

[23] S. V. Puranik, A. Keyhani, and F. Khorrami, "State-Space Modeling of Proton Exchange Membrane Fuel Cell," IEEE Transactions on Energy Conversion, vol. 25, no. 3, pp. 804–813, Sep. 2010.

[24] X. Chen, J. Xu, Q. Liu, Y. Chen, X. Wang, W. Li, Y. Ding, and Z. Wan, "Active disturbance rejection control strategy applied to cathode humidity control in PEMFC system," Energy Conversion and Management, vol. 224, p. 113389, Nov. 2020.

[25] N. Yousfi-Steiner, Ph. Moçotéguy, D. Candusso, D. Hissel, A. Hernandez, and A. Aslanides, "A review on PEM voltage degradation associated with water management: Impacts, influent factors and characterization," Journal of Power Sources, vol. 183, no. 1, pp. 260–274, Aug. 2008.

[26] S.-E. Nam, S.-O. Kim, Y. Kang, J. W. Lee, and K.-H. Lee, "Preparation of Nafion/sulfonated poly(phenylsilsesquioxane) nanocomposite as high temperature proton exchange membranes," Journal of Membrane Science, vol. 322, no. 2, pp. 466–474, Sep. 2008.

[27] T. Kim, H. Lee, W. Sim, J. Lee, S. Kim, T. Lim, and K. Park, "Degradation of proton exchange membrane by Pt dissolved/deposited in fuel cells," Korean Journal of Chemical Engineering, vol. 26, no. 5, pp. 1265–1271, Sep. 2009.

[28] A. Kusoglu, A. Kwong, K. T. Clark, H. P. Gunterman, and A. Z. Weber, "Water Uptake of Fuel-Cell Catalyst Layers," Journal of The Electrochemical Society, vol. 159, no. 9, p. F530, Aug. 2012.

[29] M. A. Barique, E. Tsuchida, A. Ohira, and K. Tashiro, "Effect of Elevated Temperatures on the States of Water and Their Correlation with the Proton Conductivity of Nafion," ACS Omega, vol. 3, no. 1, pp. 349–360, Jan. 2018.

[30] J. Lu, B. Sun, D. Huang, T. Gu, P. Wang, and W. Li, "Parameter Design of Core Components of Proton Exchange Membrane Fuel Cell (PEMFC) for Commercial Vehicles," IAENG International Journal of Applied Mathematics, vol. 53, no. 1, pp. 1–8, Mar. 2023.

[31] Z. Liu and H. He, "Sensor fault detection and isolation for a lithium-ion battery pack in electric vehicles using adaptive extended Kalman filter," Applied Energy, vol. 185, pp. 2033–2044, Jan. 2017.

[32] L. Dongping, Y. Yingchun, S. Shikai, H. Jun, S. Haoru, Y. Qiang, H. Sunyan, and D. Fei, "Research on Fault Diagnosis based on Improved Generative Adversarial Network under Small Samples," IAENG International Journal of Computer Science, vol. 50, no. 1, pp. 1–7, Mar. 2023.

Katherin Indriawati was born in East Java, Indonesia, on 23 May 1976. She received a B.Eng in Engineering Physics and an M.Eng frInstrumentation and Control, Institut Teknologi Bandung (ITB), Bandung, Indonesia, in 1998 and 2005, respectively. She graduated with a doctoral degree in electrical engineering at Institut Teknologi Sepuluh November (ITS), Surabaya, Indonesia, in 2016. Currently, she is a professor at Engineering Physics, ITS in the field of modern control systems. She is the author of more than 50 articles. Her research interests include supervisory control, fault-tolerant control, fault detection, diagnosis, and decision-making schemes.

Tasya Y. Christnantasari. received B.Eng degree in engineering physics from Institut Teknologi Sepuluh Nopember, Indonesia in 2021 and M.Sc degree in control and optimisation from Imperial College London, U.K. in 2023. During her studies, she mastered programming using Matlab, Python, and C++ and obtained some national scholarships from the Indonesian government. Her research interests include distributed state estimation, multi-agent control, fault detection and isolation, and differential algebraic equation (DAE) analysis as well as their application to large-scale systems such as water networks and robot manipulators.

Nur Laila Hamidah was born on 10th July 1988 in Jombang, Indonesia. She received her B.Eng from Engineering Physics, ITS in 2010, and her M.Sc from the Graduate Institute of Applied Science and Technology, National Taiwan University of Science and Technology (NTUST) in 2013. She graduated with a doctoral degree in advanced technology from Kumamoto University, Japan in 2020. Currently, she is an assistant professor at Engineering Physics, ITS in the field of membrane technology for electrochemical devices. She got an award as a Young Scientist at the 2019 Asian Conference of Chemical Sensors. Her research interests include solid polymer electrolytes for electrochemical devices, biofuel production from waste and fungi, and battery management systems.